

# Realizing the driven nonlinear Schrödinger equation with stationary light

Priyam Das,<sup>1</sup> Changsuk Noh,<sup>1</sup> and Dimitris G Angelakis<sup>1,2,\*</sup>

<sup>1</sup>Centre for Quantum Technologies, National University of Singapore, 3 Science Drive 2, Singapore 117543

<sup>2</sup>Science Department, Technical University of Crete, Chania, Crete, Greece, 73100

A tunable optical waveguide system to simulate the nonlinear Schrödinger equation (NLSE) with a periodic lattice potential in an out-of-equilibrium scenario is proposed. The system is formally similar to other nonlinear systems such as Bose-Einstein condensates in optical lattices or electromagnetic fields propagating in conventional Kerr-nonlinear optical media. We discuss the advantages of the proposed system compared to these systems and investigate the transport properties in both the linear and nonlinear regimes. Multistable behaviour and a novel horizontal peak in the transmission spectrum is observed in the nonlinear regime, the latter near a band-gap region introduced by the periodicity. The proposed model provides an excellent testbed to study out-of-equilibrium NLSE dynamics due to the ease of introducing a coherent source (an input laser field), the extra control over the sign and strength of nonlinearity and the freedom in choosing the shape and depth of the underlying potential. As we discuss in detail, our proposal is within reach of experimental implementation.

PACS numbers: 42.50.Gy,05.60.Cd,42.65.Pc

## I. INTRODUCTION

Nonlinear Schrödinger equation (NLSE) arises naturally in many areas of physics. For example, it describes propagation of an electromagnetic field in a nonlinear medium [1] or the interacting ground state of a Bose-Einstein condensate where the equation goes by the name of Gross-Pitaevskii equation [2]. Recently, it has been shown that the equation also governs the dynamics of stationary photons in a nonlinear optical fibre setup [3], where strong interaction between photons are induced using enhanced Kerr nonlinearities obtained by electromagnetically induced transparency (EIT) [4].

One of the interesting properties to study in systems governed by NLSE is nonlinear transport properties. Examples include nonlinear transport of Bose-Einstein condensates [5–8] and soliton propagation in nonlinear optics [1, 9]. Photonic transfer in a nonlinear optical fibre set-up based on EIT has also been studied [10], but unlike in the previous examples, the study focuses on the regime of strongly interacting few-quanta without a potential. This nonlinear optical fibre system is an example of driven-dissipative systems that has attracted a lot of interest recently (see, for example, [11–13]), and is naturally operated out of equilibrium. It is therefore an excellent system to study the nonequilibrium physics such as the transport properties.

In the present work, we study, in the semiclassical limit, the transport of photons inside a strongly nonlinear waveguide of length  $L$  depicted in Fig. 1 (a). The semiclassical regime is likely to be the starting point of experimental investigations which could be used not only to study the physics in the regime, but also to extract relevant parameters of the system for example.

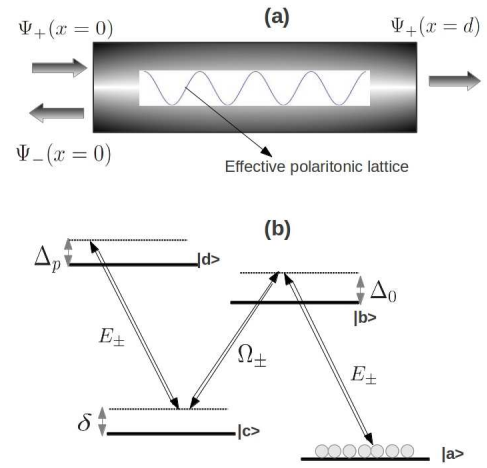


Figure 1: a) Schematic diagram of the system, describing the quantum transport in an effective polaritonic lattice inside a waveguide. b) A Level diagram showing various detunings and coupling between the fields and levels.

Taking advantage of the tunability of quantum optical systems based on EIT, one can vary the effective mass and the interaction parameters over a wide range of values. In particular, we introduce a periodic lattice potential in the NLSE following the proposal of [14]. The proposed system thus allows the study of transport properties in a specific periodic nonlinear system which has not been studied in detail before. As an example of a nonlinear phenomena we investigate bistability behaviour in the transmission spectrum that have been well-studied in other nonlinear systems.

The system studied in this work is formally similar to a Bose-Einstein condensate (BEC) in an optical lattice [15] and also systems studied in nonlinear optics [1, 9, 16]. It therefore provides a new versatile platform to study transport properties of the NLSE equation arising

\*Electronic address: dimitris.angelakis@gmail.org

in different physical systems, with several advantages. To name a few before we discuss them in more detail later, the platform allows more efficient measurement of the output states optically, a more natural implementation of a coherent source (the drive) and extra control in the shape of the potential.

Finally, we note that the nonlinear optical fiber system allows the study of quantum transport properties of interacting bosons [10]. We plan to investigate such quantum transport properties with a lattice potential in future work.

## II. SYSTEM

The nonlinear waveguide system investigated in this work is based on the four level EIT scheme. A schematic digram of the four level configuration and the coupling between the fields and levels are shown in Fig. 1(b). The quantum fields  $E_{\pm}$  couple the ground state  $|a\rangle$  and an excited state  $|b\rangle$ . A metastable state  $|c\rangle$  is coupled to  $|b\rangle$  through two classical counter-propagating fields of Rabi frequencies  $\Omega_{\pm}$ . The nonlinearity is introduced in the system by adding an additional state  $|d\rangle$ , which is coupled to  $|c\rangle$  through the quantum fields  $E_{\pm}$ . Earlier related proposals [3, 10, 14, 17, 18] were based on a hollow core fiber filled with ultracold atoms [19–24]. However, another 1D waveguide system, tapered fiber, coupled with an ensemble of atoms has been demonstrated recently [25, 26] and the authors feel that the both are promising systems to realize the particular Kerr-nonlinear photonic system considered in this work.

Following the methods described in [3, 10], we define dark-state polariton operators which, in the slow light limit, are written as  $\hat{\Psi}_{\pm} = g\sqrt{2\pi n_0}\hat{E}_{\pm}/\Omega_{\pm}$ . Here,  $n_0$  is the mean density of an ensembles of atoms coupled to the waveguide and  $g$  is the atom-field coupling strength. For simplicity, we restrict ourselves to the case where the Rabi frequencies of the control fields are equal:  $\Omega_{\pm} = \Omega$ .

Introducing the symmetric and anti-symmetric combinations of the polariton operators  $\Psi = \frac{\Psi_+ + \Psi_-}{\sqrt{2}}$  and  $A = \frac{\Psi_+ - \Psi_-}{\sqrt{2}}$ , it is easily seen that, in the limit of large optical depth,  $A$  adiabatically follows  $\Psi$ :  $A = -ik_0L_{coh}\frac{m_R}{m}\partial_z\Psi$ . Here,  $m$  is the complex effective mass,  $m_R$  is the real part of  $m$ ,  $k_0$  is the wave vector of the lattice potential and  $L_{coh}$  is the coherence length introduced in [10]. The specific forms of these parameters, and other effective interaction parameters to be introduced below, in terms of bare optical parameters are provided in Appendix A.

As shown in [14], we introduce a polaritonic lattice potential in the above setup by creating a periodic modulation in the atomic density in the ground state  $|a\rangle$ :  $n_a = n_0 + n_1 \cos^2(k_0z)$ . The dynamics of the symmetric polariton operator is governed by the nonlinear Schrödinger equation with a lattice potential,

$$i\partial_t\Psi = -\frac{1}{2m}\partial_z^2\Psi + 2V\cos^2(k_0z)\Psi + 2\chi\Psi^\dagger\Psi^2, \quad (1)$$

where,  $V$  is an effective lattice depth and  $\chi$  is an effective polariton-polariton interaction strength. After substituting in  $\Psi(z, t) = \psi(z, \epsilon)e^{-i\epsilon t}$ , the above equation reduces to a dimensionless form:

$$-\partial_{\bar{z}}^2 + \frac{m}{m_R}(\bar{V} - \bar{\epsilon} + \bar{V}\cos(2\bar{z}) + 2\bar{\chi}\psi^\dagger\psi)\psi = 0, \quad (2)$$

where,  $z, \psi$  and  $V$  has been scaled by  $1/k_0, \sqrt{k_0}$  and the recoil energy  $E_R = k_0^2/(2m_R)$ , respectively. In terms of the right and left propagating fields  $\psi_+$  and  $\psi_-$ , Eq. (2) can be decomposed into the following coupled mode equations:

$$\partial_{\bar{z}}\psi_+ - \frac{i}{2}\frac{m}{l_{coh}m_R}(\psi_+ - \psi_-) - \frac{il_{coh}}{2}[\bar{\epsilon} - \bar{V} - \bar{V}\cos(2\bar{z}) - \frac{\bar{\chi}}{2}(\psi_+ + \psi_-)^\dagger(\psi_+ + \psi_-)](\psi_+ + \psi_-) = 0, \quad (3)$$

$$\partial_{\bar{z}}\psi_- - \frac{i}{2}\frac{m}{l_{coh}m_R}(\psi_+ - \psi_-) + \frac{il_{coh}}{2}[\bar{\epsilon} - \bar{V} - \bar{V}\cos(2\bar{z}) - \frac{\bar{\chi}}{2}(\psi_+ + \psi_-)^\dagger(\psi_+ + \psi_-)](\psi_+ + \psi_-) = 0, \quad (4)$$

with  $l_{coh} = k_0L_{coh}$  quantifies the ratio between the coherence length and the lattice constant.

In passing, we remark that the above coupled mode equations are similar to the nonlinear coupled mode equations arising in the study of nonlinear wave propagation in one-dimensional periodic structures [16].

Equation (2) is equivalent to the Gross-Pitaevskii equation with an optical lattice potential. While transport problems in BEC have been studied extensively [5–8], the present study differs from the BEC systems in several ways. One of the important differences is that the non-equilibrium driving conditions arises much more naturally in the present system. Preparing a coherent source of BEC is much more difficult compared to a coherent source of photons, i.e., a laser. Another is that we study transport properties in a sinusoidal lattice potential equivalent to an optical lattice potential, whereas in the BECs, transport studies are often limited to a single or double well potentials, or for a periodic delta function potential that are analytically tractable.

It is perhaps helpful here to mention that, unlike other nonlinear systems mentioned earlier, two periodicities are present in the current optical system. The first one is due to counter-propagating control fields creating stationary excitations [27, 28] and the second one, created by the modulated atomic density, provides the periodic potential in the NLSE shown in Eq. (1).

Following Hafezi *et al.* [10], we specify the boundary conditions  $\psi_+(z=0) = \alpha$  and  $\psi_-(z=d) = 0$ , where  $\alpha$  is the field strength for the driving laser impinging from the left and  $d = k_0L$  is the dimensionless length of the waveguide. This represents a situation depicted in Fig. 1(a) where the only input field impinges on the waveguide from the left. The transmission spectra, i.e., the transmittivity as a function of the probe field detuning  $\bar{\epsilon}$ , is investigated for both linear and nonlinear regimes in the semiclassical limit and especially the effects of the

lattice potential is explored. Detuning the probe field corresponds to detuning the quantum fields which can be easily implemented in experiments. Consequences of this detuning is discussed in Appendix B.

### III. LINEAR REGIME

If the nonlinearity is assumed to be zero, Eq. (2) is equivalent to Mathieu's differential equation with well known solutions. In this section, we plot the transmission spectra obtained from these solutions. The lattice potential introduces bandgaps and bound states and shifts the resonance peaks in the transmission spectrum. Incidentally, locations of these band gaps can be calculated easily from the imaginary part of the Mathieu Characteristic Exponent as shown in Appendix C.

Before we show you the transmission spectrum, we would like to point out that the linear case can be achieved without the 4th level in Fig. 1b, which makes experiments easier [28]. In the linear case, one is able to study experimentally a classic transmission problem of a quantum particle through a potential. To put it another way, using the periodic optical medium it is possible to build a tunable optical experiment to simulate the Schrödinger equation in a controlled environment. The shape of the potential can also be varied to test other classic text-book problems by changing the atomic density distribution.

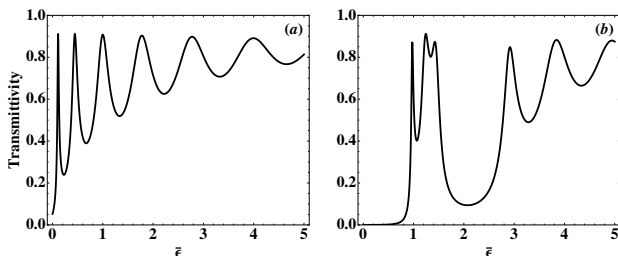


Figure 2: Transmission spectra for  $l_{coh} = 0.25$ ,  $d = 3\pi$ ,  $\beta = 12\pi/50 \approx 0.75$ ,  $\bar{V} = 0$  (a) and  $\bar{V} = 1.0$  (b). The bound state and the first band gap is clearly shown in (b).

Figure 2 shows the transmittivity as a function of the input field detuning for two different values of  $\bar{V}$  for  $l_{coh} = 0.25$  with total loss determined by  $\beta = (d/l_{coh})(\Gamma/|\Delta_0|) = 12\pi/50 \approx 0.75$ . Bare optical parameters corresponding to these effective parameters are given in Appendix A, where it is shown that the magnitude of  $\bar{V}$  can be changed by tuning  $\Delta_p$ . The values were carefully chosen such that the phenomena depicted in this work are within reach of experimental investigation.

When  $\bar{V} = 0$ , there are perfect transmissions at resonances  $\bar{\epsilon}_0 = (n\pi)^2$  for  $n = 1, 2, 3, \dots$  and at an additional point  $\bar{\epsilon}_0 = 1$ . These transmission resonances are an artefact of an effective cavity produced by counter-propagating control fields. For non-zero  $\bar{V}$ , a continuum exists after  $2\bar{V}$  (maximum potential height) as expected,

but there are additional resonances for  $\bar{\epsilon} < 2\bar{V}$  signifying bound states that exist due to the potential. The energy of the first bound state can be readily calculated within the perturbation theory as  $\bar{V} - \bar{V}^2/8$ , which matches the starting point of the first resonance in the figure. Furthermore, the location of other resonances can be approximated from a generalization of the free field resonance points  $d\sqrt{\bar{\epsilon}} = n\pi$  to  $d\sqrt{\bar{\epsilon} - \bar{V} + \bar{V}^2/8} = n\pi$ , such that only the quasi-kinetic energy part is used to determine the resonance condition. This approximation works well for  $\bar{\epsilon} \gg \bar{V}$ , i.e., when the effect of the potential is only perturbative and the solution is expected to be close to the free field case. It can be easily seen that this expression matches the resonances for  $\bar{\epsilon} > 2\bar{V}$ .

### IV. NON-LINEAR REGIME

In this section, we study the effects of the nonlinearity and the lattice potential on the transport properties. As remarked earlier, the nonlinear transport problem with a potential has been studied in detail in various physical systems. For example, Paul *et. al.* and Rapedius *et. al.* have studied similar nonlinear barrier transmission problems for BECs, where they showed the bistability in the transmission spectrum [5–8]. However, the present system offers unique advantages over the previous works: tunability of the parameters, large nonlinearity and readily available coherent sources. There are many interesting phenomena in the non-linear regime, but in this work we focus on the bistability (or multistability) as a typical phenomenon in nonlinear systems. We choose the parameters used in the previous section and  $Re(\bar{\chi}) = \pm 0.02$  and  $\pm 0.05$ . The sign and the magnitude of  $\bar{\chi}$  can be tuned by varying the single-photon detuning  $\Delta_p$  as shown in the Appendix A.

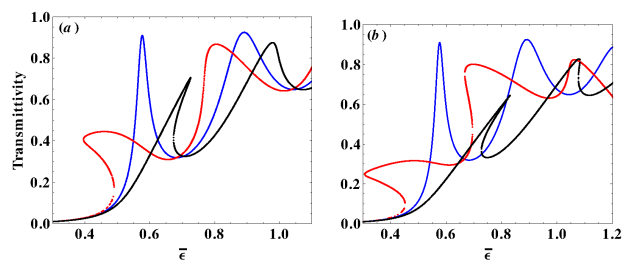


Figure 3: Transmission spectra for  $\bar{V} = 0.5$ ,  $l_{coh} = 0.25$ ,  $\alpha = 0.5$ ,  $d = 3\pi$ ,  $\beta \approx 0.75$  and three different values of  $|\bar{\chi}|$ . (a) For repulsive nonlinearity ( $\bar{\chi} = 0.02$ ), one can see the shift of the transmission peaks to the right (black curve). For attractive nonlinearity ( $\bar{\chi} = -0.02$ ), the shift is in the opposite direction (red curve). (b) Effect of the nonlinearity on transmission spectra is shown for  $\bar{\chi} = 0.05$  (black curve) and  $\bar{\chi} = -0.05$  (red curve). The blue curve depicts the transmittivity for  $\bar{\chi} = 0$ .

Figure 3 shows the effects of repulsive and attractive nonlinearity on the transmission spectrum. For repulsive

nonlinearity (black curves), one can see the shift of the transmission resonances to the right, whereas for attractive nonlinearity (red curves) the shift is in the opposite direction. The nonlinear shift induces strong bistability in the first peak. The suppression of the transmission peaks is due to the presence of nonlinear loss absent in the linear case. Increasing the magnitude of nonlinearity of course causes larger nonlinear shift and more loss. In Fig. 3(b) the shift is sufficient to make the second resonance of the repulsive case overlap with the third resonance of the attractive case. Further increase in the nonlinearity for the attractive case results in the transmission peaks disappearing to the left. This phenomenon signifies the shift of the transmission peak from the resonance state to a bound state at  $\bar{\epsilon} < 0$  [6].

Fixing  $\bar{\chi}$  and increasing the input field strength  $\alpha$  has similar effects on the transmission spectrum to fixing  $\alpha$  and increasing  $\bar{\chi}$ . This is expected because the effective nonlinearity determining the nonlinear shift is determined by  $\bar{\chi}|\bar{\psi}|^2$ , where the overbar denotes averaging, and  $|\bar{\psi}|^2$  of course depends on  $\alpha$ .

Having observed the nonlinear shifts and bistability, we investigate the effect of the lattice potential on these nonlinear effects. We concentrate on the repulsive case for this purpose. Figure 4 depicts the scenario for three different values of  $\bar{V} = 0.1, 0.5$  and  $1.0$ .

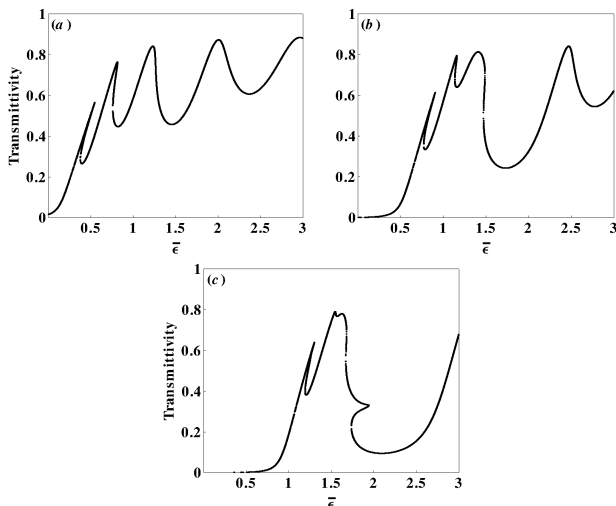


Figure 4: Transmission spectra for  $l_{coh} = 0.25$ ,  $\alpha = 1.0$ ,  $\bar{\chi} = 0.02$ ,  $d = 3\pi$  and  $\beta \approx 0.75$ . (a), (b) and (c) correspond to  $\bar{V} = 0.1, 0.5$  and  $1.0$  respectively. (c) shows an interesting behaviour near  $\bar{\epsilon} = 2$ . A horizontal peak, near the bandgap region, arises due to an interplay between lattice potential and nonlinearity.

As  $\bar{V}$  increases, the transmission spectrum shifts towards the higher value of  $\bar{\epsilon}$ . The constant shift is due to the constant part of the potential which shifts the energy and the reduced transmittivity of the third peak results from the development of a band gap. This shift and the development of the band means that the resonance peaks get pushed towards each other as  $\bar{V}$  increases. Near

$\bar{V} = 1.0$ , the second and the third peak merges and a peculiar feature is observed between  $\bar{\epsilon} = 1.5$  and  $\bar{\epsilon} = 2.0$ : a horizontal peak near the bandgap region appears, as seen in Fig. 4(c). As far as the authors are aware, this horizontal peak has not been observed before and is a unique feature arising due to an interplay between the nonlinearity and the band-gap effect of the lattice potential. We have verified that this feature is more pronounced for extreme parameters and its development is under investigation.

Finally, we remark that not all of the multiple solutions are stable. Normally the solution corresponding to the negative slope is unstable and the system shows bistable behaviour. To show which part of the transmittivity curve is occupied one has to study the dynamics of the system as in [5] for example. A hysteresis behaviour can then be observed as a relevant parameter is varied in time. In this way a connection to the swallow-tail behaviour discussed in the BEC literature can be made through a general argument given by Mueller [29].

## V. CONCLUSION

We have studied a nonlinear optical system based on EIT and showed that this system is useful for studying linear and nonlinear transport properties. In the linear case, the system provides a clean and tunable laboratory realization of a textbook quantum transport problem. In the nonlinear case, the system allows the study of the transport problem in an optical lattice, similar to that studied in the context of a BEC in an optical lattice. Transport is a lot easier to investigate in the proposed optical system, due to the ease of preparing a coherent source compared to the BEC case. Transmission spectrum have been studied for various regimes of parameters and properties such as band gap and multistable behaviour have been demonstrated. The authors believe the prevalence of the nonlinear Schrödinger equation studied in this work and the non-equilibrium driven-dissipative nature of the system makes the work interesting to a broad audience.

## Acknowledgement

We would like to acknowledge the financial support provided by the National Research Foundation and Ministry of Education, Singapore. PD thanks Dr. J. Bandyopadhyay for many useful discussion.

## Appendix A: Experimental feasibility

Various effective parameters appearing in Eq. (2) and below can be written in terms of bare optical parameters

as

$$L_{coh} = \frac{|\Delta_0|^2 + (\Gamma/2)^2}{\Gamma_{1D} n_0 |\Delta_0|}, \quad (A1)$$

$$m = -\frac{\Gamma_{1D} n_0}{4\nu_g (\Delta_0 + i\Gamma/2)}, \quad (A2)$$

$$E_R = \frac{k_0^2}{2m_R}, \quad (A3)$$

$$\bar{V} = \frac{\Lambda \Gamma_{1D}^2 \delta n_0 n_1 |\Delta_0|}{8\Omega^2 k_0^2 (\Delta_0^2 + \Gamma^2/4)}, \quad (A4)$$

$$\begin{aligned} \bar{\chi} &= \frac{\Lambda^2 \Gamma_{1D}^2 n_0 |\Delta_0|}{4(|\Delta_0|^2 + \Gamma^2/4) k_0 (\Delta_p + i\Gamma/2)} \\ &= \frac{\Lambda^2 \Gamma_{1D} \Delta_p}{4l_{coh} (\Delta_p^2 + \Gamma^2/4)} \left(1 - i \frac{\Gamma}{2\Delta_p}\right), \end{aligned} \quad (A5)$$

where  $\Lambda = \Omega^2 / (\Omega^2 - \delta\Delta_0/2)$ ,  $\Gamma_{1D}$  denotes the spontaneous emission rate into the guided modes and  $\Gamma$  the total spontaneous emission rate from the excited states  $|b\rangle$  and  $|d\rangle$  assumed to be the same for simplicity. The detunings are shown in Fig. 1 (b) and the last line follows immediately from  $l_{coh} = k_0 / (4m_R \nu_g)$ . Thus, to get a large nonlinearity  $l_{coh}$  has to be small, because to suppress losses it has been assumed that  $|\Delta_p| \gg \Gamma > \Gamma_{1D}$ .

In the main text, we fix the value of the nonlinearity  $\bar{\chi}$ . Once this is done, the value of  $\bar{V}$  can be changed according to the ratio:

$$\frac{\bar{V}}{\bar{\chi}} = \frac{|\delta| |\Delta_p| n_1}{2\Omega^2 k_0 \Lambda}. \quad (A6)$$

We will assume the parameters mostly similar to those used in [14]; all the frequencies are in units of the spontaneous emission rate which we take to be  $\Gamma = 10 \text{ Mhz}$  for simplicity.  $\delta = -0.01$ ,  $\Delta_0 = -50$ ,  $\Gamma_{1D} = 0.2$ ,  $n_0 = 10^7 m^{-1}$ ,  $n_1 = 10^6 m^{-1}$ ,  $k_0 = 10^4 m^{-1}$ . With these values we obtain

$$\begin{aligned} l_{coh} &= 0.25, \\ \bar{V} &= \frac{1}{10(\Omega^2 - 0.25)}, \\ \bar{\chi} &= \left(1 - i \frac{1}{2\Delta_p}\right) \frac{0.2\Delta_p \Lambda^2}{\Delta_p^2 + 1/4}. \end{aligned}$$

Values of the real part of  $\bar{\chi}$  ( $\bar{\chi}_R$ ) and  $\bar{V}$  as functions of  $\Delta_p$  and  $\Omega$  are plotted in Fig. 5.

### Appendix B: Probe field detuning

With the numbers used in the previous section, we deduce that  $E_R \approx 5 \times 10^{-3} \Gamma$ , assuming that  $\nu_g = 100 m s^{-1}$ . Because the recoil energy is several orders of magnitudes smaller than the one photon detunings, one can safely ignore the contributions to the one photon detunings due to the probe field detuning. One cannot, however, arbitrarily increase the two-photon detuning to explore the spectrum, because if the two-photon detuning is too large, the

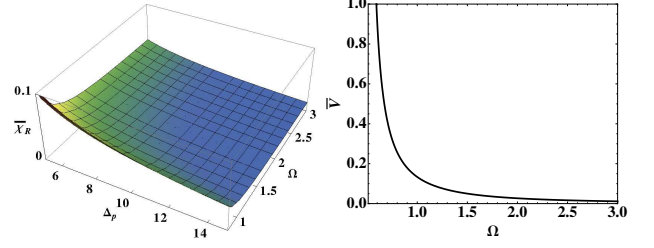


Figure 5: Plots of (a) the real part of the interaction parameter  $\bar{\chi}_R$ , as a function of one photon detuning  $\Delta_p$ . (b) The lattice depth as a function of Rabi frequency  $\Omega$ . Here, both  $\Delta_p$  and  $\Omega$  are in terms of  $\Gamma$ .

two-photon resonance condition breaks and EIT works no more. The two photon resonance condition is  $\Omega^2 \gg |\delta\Gamma|$ , where  $\delta$  is the two photon detuning. Thus, one will have to modify the frequency of the control laser to keep  $\delta$  within the EIT regime. We will assume that this is the case in this work.

### Appendix C: Mathieu characteristic exponent

As mentioned in Sect. III the locations of the bandgaps can be found from the Mathieu characteristic exponent (MCE), where the imaginary part is non-zero at band gaps. This follows from the fact that all Mathieu functions  $F(a, q, z)$  can be written in the form  $e^{i\mu z} P(a, q, z)$ , with  $P(a, q, z)$  periodic in  $z$ . As an example we plot the transmittivity and the imaginary part of the MCE for  $\bar{V} = 2$ ,  $d = 3\pi$  and  $l_{coh} = 0.1$  in Fig. 6 shows. Finite length of the potential causes the small non-zero transmissions seen at the band gap.

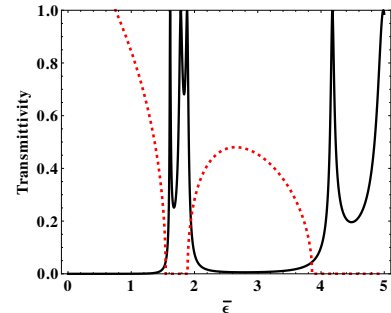


Figure 6: Transmittivity (blue solid line) and the imaginary part of Mathieu Characteristic Exponent (red dotted curve) for  $\bar{V} = 2$ ,  $d = 3\pi$  and  $l_{coh} = 0.1$ . MCE predicts the band gaps quite well even for the relatively short waveguide length used.

- 
- [1] Boyd R W 1992 *Nonlinear Optics* (Academic Press, London)
- [2] Pitaevskii L and Stringari S 2003 *Bose-Einstein Condensation* (Clarendon, Oxford)
- [3] Chang D E *et al* 2008 *Nature Phys.* **4** 884-9
- [4] Schmidt H and Imamoglu A 1996 *Opt. Lett.* **21** 1936
- [5] Paul T, Klaus R and Schlagheck P 2005 *Phys. Rev. Lett.* **94** 020404
- [6] Rapedius K, Witthaut D and Korsch H J 2006 *Phys. Rev. A* **73** 033608
- [7] Paul T, Hartung M, Klaus R and Schlagheck P 2007 *Phys. Rev. A* **76** 063605
- [8] Rapedius K and Korsch H J 2008 *Phys. Rev. A* **77** 063610
- [9] Christodoulides D N and Joseph R I 1989 *Phys. Rev. Lett.* **62** 1746
- [10] Hafezi M, Chang D E, Gritsev V, Demler E A and Lukin M D 2011 *Europhys. Lett.* **94** 54006, 2012 *Phys. Rev. A* **85** 013822
- [11] Diehl S *et al* 2008 *Nature Phys.* **4** 878
- [12] Verstraete F, Wolf M M and Cirac J I 2009 *Nature Phys.* **5** 633
- [13] Carusotto I, Gerace D, Tureci H E, Liberato S De, Ciuti C, and Imamoglu A 2009 *Phys. Rev. Lett.* **103** 033601
- [14] Huo M-X and Angelakis D G 2012 *Phys. Rev. A* **85** 023821
- [15] Morsch O and Oberthaler M 2006 *Rev. Mod. Phys.* **78** 179
- [16] Goodman R H, Weinstein M I and Holmes P J 2001 *J. Nonlinear Sci.* **11** 123
- [17] Angelakis D G, Huo M-X, Kyoseva E and Kwek L C 2011 *Phys. Rev. Lett.* **106** 153601
- [18] Shahmoon E, Kurizki G, Fleischhauer M and Petrosyan D 2011 *Phys. Rev. A* **83** 033806
- [19] Ghosh S, Sharping J E, Ouzounov D G and Gaeta A L 2005 *Phys. Rev. Lett.* **94** 093902
- [20] Nayak K P *et al* 2007 *Opt. Express* **15** 5431-8
- [21] Takekoshi T and Knize R J 2007 *Phys. Rev. Lett.* **98** 210404
- [22] Christensen C A *et al* 2008 *Phys. Rev. A* **78** 033429
- [23] Vorrath S, Möller S A, Windpassinger P, Bongs K and Sengstock K 2010 *New J. Phys.* **12** 123015
- [24] Bajcsy M *et al* 2011 *Phys. Rev. A* **83** 063830
- [25] Nayak K P *et al* 2007 *Opt. Express* **15** 5431-8
- [26] Vetsch E *et al* 2010 *Phys. Rev. Lett.* **104** 203603
- [27] André A and Lukin M D 2002 *Phys. Rev. Lett.* **89** 143602
- [28] Bajcsy M, Zibrov A S and Lukin M D 2003 *Nature* **426** 638
- [29] Mueller E J 2002 *Phys. Rev. A* **66** 063603